Progress In Electromagnetics Research, Vol. 135, 411–433, 2013

OPTIMIZATION OF THE E-PLANE LOADED RECTANGULAR WAVEGUIDE FOR LOW-LOSS PROPAGATION

Daniel Sanchez-Escuderos*, Miguel Ferrando-Bataller, Jose I. Herranz, and Mariano Baquero-Escudero

Instituto de Telecomunicaciones y Aplicaciones Multimedia, Univertitat Politècnica de València, c/ Cami de Vera s/n, Valencia 46022, Spain

Abstract—The insertion of vertical slabs in a metallic rectangular waveguide distorts the power distribution of the waveguide, producing new modes and modifying the existing ones. The resulting waveguide, known as E-plane loaded rectangular waveguide, is studied in this paper, focusing the attention on the TE-type modes in a symmetrical case. A quasi-TE_{10} is found which may confine the energy in the central air region by suitably choosing the dielectric slabs' dimensions. An algorithm to optimize these dimensions is proposed in order to maximize the confinement of power in the air region and minimize the attenuation of the mode. This minimization is specially important at high frequencies, where the ohmic losses and the dielectric absorption become extremely high. This paper includes an example at THz frequencies and presents the design of several devices using the E-plane loaded rectangular waveguide.

1. INTRODUCTION

Partially filled rectangular waveguides have been extensively studied in the literature [1, 2] due to their wide range of applications, e.g., matching transformers, phase shifters [3] or electromagnetic material characterization [4]. These kind of waveguides may be divided into two main types: E-plane loaded rectangular waveguides [5–8] and H-plane loaded rectangular waveguides [9, 10].

E-plane loaded rectangular waveguides contain dielectric slabs parallel to the narrow wall and extending the full height of the

Received 23 October 2012, Accepted 20 December 2012, Scheduled 26 December 2012

* Corresponding author: Daniel Sanchez-Escuderos (dasanes1@iteam.upv.es).

waveguide. In general, the number and material of the different slabs, and the separation between them, are arbitrary [6, 7], allowing the waveguide to be designed for a wide range of applications and frequencies.

The modal analysis of this waveguide finds hybrid modes with regard to the longitudinal direction. These modes may be classified as Longitudinal Section Electric Modes (LSE), with a transversal component of the electric field vanishing, e.g., $E_x = 0$, and Longitudinal Section Magnetic Mode (LSM), with the same vanishing transversal component but for the magnetic field ($H_x = 0$). According to Harrington's notation [2], LSE modes can also be noted as TE^x, and LSM modes as TM^x. In this paper, this last notation is adopted.

Both modes have been studied previously in [7] for N symmetrical slabs and in [6] for a general configuration. This paper is focused on the study of a particular case formed by the insertion of 2 dielectric slabs in a rectangular waveguide, placed symmetrically with regard to the waveguide centerline [5]. Under this configuration, low-order TE^x modes are dominant [7].

The proposed configuration presents an interesting characteristic. If materials and dimensions of the different slabs are suitably chosen, one of the first TE^x modes (TE^x_{30}) is able to confine the energy in the central region. This mode is a quasi-TE_{10} mode since it presents an amplitude distribution similar to that of the fundamental mode in a conventional rectangular waveguide.

By confining the energy in the central region and choosing low-loss materials, the attenuation of the TE^x_{30} mode may become lower than the attenuation of the fundamental mode in the equivalent rectangular waveguide. This characteristic is specially important at high frequencies, e.g., submillimeter-wave or THz frequencies. At these frequencies, waveguides are affected by severe conductor skin-depth losses and dielectric absorption [11], which considerably increases the attenuation of the waveguides [12]. Hence, the confinement of power in a region of air by non-conducting materials may decrease noticeably the attenuation of the waveguide. The resulting structure may be specially useful in highly sensitive applications [13], in the design of horn antennas with an enhanced efficiency [14] or in near-field probing systems [15].

The aim of this paper is to present an algorithm to efficiently determine the dimensions of the dielectric slabs in the E-plane loaded rectangular waveguide to maximize the power confinement of TE^x_{30} mode. Taking advantage of this confinement, this paper shows that the proposed waveguide also presents low losses on curves [11, 16], and can be used to design efficient devices.

The paper is organized as follows: firstly, the TE^x modes of the E-plane loaded waveguide are analytically studied and both, conductor and dielectric losses are obtained. Then, the algorithm to optimize the dielectric slabs is proposed and several examples, including a practical realization, are shown. Finally, the behaviour of the waveguide at high frequencies is reported and the possibility of bending the E-plane loaded rectangular waveguide and designing a directional coupler is examined.

2. E-PLANE LOADED RECTANGULAR WAVEGUIDE

The E-plane loaded rectangular waveguide under study, shown in Fig. 1, is a rectangular waveguide with dimensions $w \times h$. The waveguide is divided into 5 different regions. The central region (w_{a0}) and the lateral regions (w_{a1}) are filled with air, whereas the intermediate regions (w_d), in dark gray in Fig. 1, are dielectric slabs with permittivity ε_r loading the waveguide.

The described waveguide cannot be analysed using TE^z and TM^z modes, and a combination of both, the so-called *hybrid* modes, must be used instead [7]. To simplify the analysis, modes transversal to the x component are normally considered. These modes are known as LSE, for which $E_x = 0$ (TE^x), and LSM (Longitudinal Section Magnetic Modes), for which $H_x = 0$ (TM^x) [1, 2].

In general, the analysis of the E-plane loaded rectangular waveguide finds both, TE^x and TM^x modes. However, as stated in [6], low-order TE^x modes are dominant in the described structure, provided that $h \ll w$. Since the aim of this paper is to maximize the confinement of a TE^x mode, only these modes are considered in the analysis.

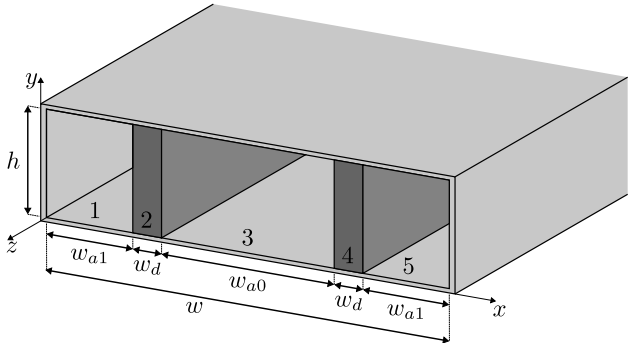

Figure 1. Symmetrical E-plane loaded rectangular waveguide.

In any region r (labeled as $r = 1$ to $r = 5$ from $x = 0$ to $x = w$) of the structure shown in Fig. 1, the electric and magnetic fields may be obtained from Maxwell's equations [2, 17] and are given by

$$E_x = 0 \qquad H_x = \left(\frac{\partial^2}{\partial x^2} + k^2\right)\psi \tag{1}$$

$$E_y = -j\omega\mu\frac{\partial\psi}{\partial z} \qquad H_y = \frac{\partial^2\psi}{\partial x\partial y} \tag{2}$$

$$E_z = j\omega\mu\frac{\partial\psi}{\partial y} \qquad H_z = \frac{\partial^2\psi}{\partial z\partial x} \tag{3}$$

where k is the wavenumber and ψ is the solution to the scalar Helmholtz equation given by

$$\nabla^2\psi + k^2\psi = 0 \tag{4}$$

The solution to the above equation is a combination of harmonic functions. By inserting this solution in expressions (1)–(3), the electric and magnetic field can be easily obtained. These fields are a general solution that must be particularized according to the boundary conditions. In the structure of Fig. 1, boundary conditions state that E_z must vanish on the upper and lower metallic walls ($y = 0$ and $y = h$) and on the lateral metallic walls ($x = 0$ and $x = w$). If boundary conditions are only applied on the upper and lower walls, the solution can be expressed as:

$$E_y^{(r)} = -\omega\mu\beta\left(A^{(r)}\cos(k_x^{(r)}x) + B^{(r)}\sin(k_x^{(r)}x)\right)\cos(k_y y)e^{-j\beta z} \tag{5}$$

$$E_z^{(r)} = -j\omega\mu k_y\left(A^{(r)}\cos(k_x^{(r)}x) + B^{(r)}\sin(k_x^{(r)}x)\right)\sin(k_y y)e^{-j\beta z} \tag{6}$$

$$H_x^{(r)} = \left(k^2 - (k_x^{(r)})^2\right)\left(A^{(r)}\cos(k_x^{(r)}x) + B^{(r)}\sin(k_x^{(r)}x)\right)\cos(k_y y)e^{-j\beta z} \tag{7}$$

$$H_y^{(r)} = -k_x^{(r)}k_y\left(-A^{(r)}\sin(k_x^{(r)}x) + B^{(r)}\cos(k_x^{(r)}x)\right)\sin(k_y y)e^{-j\beta z} \tag{8}$$

$$H_z^{(r)} = -j\beta k_x^{(r)}\left(-A^{(r)}\sin(k_x^{(r)}x) + B^{(r)}\cos(k_x^{(r)}x)\right)\cos(k_y y)e^{-j\beta z} \tag{9}$$

where $A^{(r)}$ and $B^{(r)}$ are constants, $k_y = n\pi/h$ and $k_x^{(r)}$ are determined for each region applying continuity conditions at the interface between the different regions [18–20] and boundary conditions at outer lateral metallic walls. Constants $k_x^{(r)}$ are related to k_y, β (the propagation constant) and k as:

$$k^{(r)} = \sqrt{\left(k_x^{(r)}\right)^2 + k_y^2 + \beta^2} \tag{10}$$

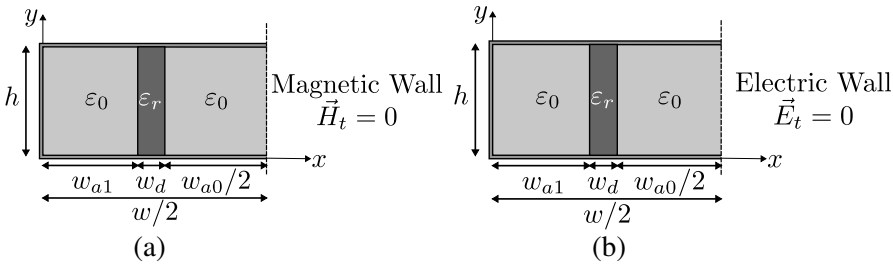

Figure 2. Application of a symmetry condition in the waveguide centerline: Separation into two subproblems. (a) Magnetic wall (even solution). (b) Electric wall (odd solution).

In region $r = 1$, the boundary condition $E_z = 0$ must be enforced at $x = 0$. By doing so, it can be easily determined that $A^{(1)} = 0$. To determine the rest of parameters, the problem is simplified assuming a symmetry plane at $x = w/2$. Thus, just half of the waveguide needs to be considered, which simplifies the computations. In order to consider all the TE^x modes, two different boundary conditions must be applied on the symmetry plane. These problems are depicted in Fig. 2.

On the one hand, if the magnetic wall condition shown in Fig. 2(a) is applied, and the continuity condition is enforced for tangential electric and magnetic field at $x = w_{a1}$ and $x = w_{a1} + w_d$, the following system is obtained:

$$\begin{bmatrix} B_1^s & -B_2^c & -B_2^s & 0 & 0 \\ k_x^{(1)}B_1^c & k_x^{(2)}B_2^s & -k_x^{(2)}B_2^c & 0 & 0 \\ 0 & B_3^c & B_3^s & -B_4^c & -B_4^s \\ 0 & -k_x^{(2)}B_3^s & k_x^{(2)}B_3^c & k_x^{(3)}B_4^s & -k_x^{(3)}B_4^c \\ 0 & 0 & 0 & -B_9^s & B_9^c \end{bmatrix} \begin{bmatrix} A^{e(1)} \\ A^{e(2)} \\ B^{e(2)} \\ A^{e(3)} \\ B^{e(3)} \end{bmatrix} = \begin{bmatrix} 0 \\ 0 \\ 0 \\ 0 \\ 0 \end{bmatrix} \quad (11)$$

where $B_1^s = \sin(k_x^{(1)}w_{a1})$, $B_2^s = \sin(k_x^{(2)}w_{a1})$, $B_3^s = \sin(k_x^{(2)}(w_{a1} + w_d))$, $B_4^s = \sin(k_x^{(3)}(w_{a1} + w_d))$, $B_9^s = \sin(k_x^{(3)}w/2)$, and B_n^c are the same expressions but substituting sine functions by cosine functions.

On the other hand, if the electric wall condition shown in Fig. 2(b) is applied, and the continuity condition is enforced at the interface between regions, the resulting system is:

$$\begin{bmatrix} B_1^s & -B_2^c & -B_2^s & 0 & 0 \\ k_x^{(1)}B_1^c & k_x^{(2)}B_2^s & -k_x^{(2)}B_2^c & 0 & 0 \\ 0 & B_3^c & B_3^s & -B_4^c & -B_4^s \\ 0 & -k_x^{(2)}B_3^s & k_x^{(2)}B_3^c & k_x^{(3)}B_4^s & -k_x^{(3)}B_4^c \\ 0 & 0 & 0 & B_9^c & B_9^s \end{bmatrix} \begin{bmatrix} A^{o(1)} \\ A^{o(2)} \\ B^{o(2)} \\ A^{o(3)} \\ B^{o(3)} \end{bmatrix} = \begin{bmatrix} 0 \\ 0 \\ 0 \\ 0 \\ 0 \end{bmatrix} \quad (12)$$

Propagation constants for modes of each problem of Fig. 2 form the complete solution of TE^x modes in the E-plane loaded rectangular waveguide shown in Fig. 1. The propagation constant (β) of each mode is determined by solving the dispersion equation. To obtain this equation, the determinant of matrices in (11), for even modes (TE^{xe}), and (12), for odd modes (TE^{xo}), is cancelled [21]. The resulting dispersion equation may be expressed for even modes as:

$$\left[\, k_x^{(1)} \cos\left(k_x^{(1)} w_{a1}\right) \;\; -\sin\left(k_x^{(1)} w_{a1}\right) \,\right][S]\begin{bmatrix} \cos\left(k_x^{(3)} w_{a0}/2\right) \\ k_x^{(3)} \sin\left(k_x^{(3)} w_{a0}/2\right) \end{bmatrix} = 0 \quad (13)$$

and for odd modes as:

$$\left[k_x^{(1)} \cos\left(k_x^{(1)} w_{a1}\right) \;\; -\sin\left(k_x^{(1)} w_{a1}\right)\right][S]\begin{bmatrix} \sin\left(k_x^{(3)} w_{a0}/2\right) \\ -k_x^{(3)} \cos\left(k_x^{(3)} w_{a0}/2\right) \end{bmatrix} = 0 \quad (14)$$

where the matrix $[S]$ is given by:

$$[S] = \begin{bmatrix} \cos\left(k_x^{(2)} w_d\right) & -\dfrac{1}{k_x^{(2)}} \sin\left(k_x^{(2)} w_d\right) \\ k_x^{(2)} \sin\left(k_x^{(2)} w_d\right) & \cos\left(k_x^{(2)} w_d\right) \end{bmatrix} \quad (15)$$

Once the propagation constant of each mode is determined, constants $A^{e,\,o(r)}$ and $B^{e,\,o(r)}$ on each region can be easily obtained by solving (11) and (12). To do so, one column of the matrices is placed as an independent term and one row must be removed due to redundancy. As a result, a 4×4 equation system is found. This system must be finally solved to determine constants $A^{e,\,o(r)}$ and $B^{e,\,o(r)}$.

Example

The above method has been implemented to obtain the propagation constants of an E-plane loaded rectangular waveguide with dimensions: $w_{a0} = 22.86\,\mathrm{mm}$, $w_{a1} = 8\,\mathrm{mm}$, $w_d = 4\,\mathrm{mm}$ and $h = 10.16\,\mathrm{mm}$, and permittivity $\varepsilon_r = 2.2$. Fig. 3 shows the obtained dispersion diagram for the TE^x modes.

Low-order modes (TE_{20}^{xe} and TE_{20}^{xo}) concentrate the energy inside the dielectric slabs (regions $r = 2$ and $r = 4$), whereas high-order modes (TE_{30}^{xe}, TE_{40}^{xo}, etc.) spread the energy across all regions. Nevertheless, it must be noted that mode TE_{30}^{xe} concentrates significantly the energy in the central region ($r = 3$). These differences may be observed in Fig. 4, which shows the field distribution for 4 different modes.

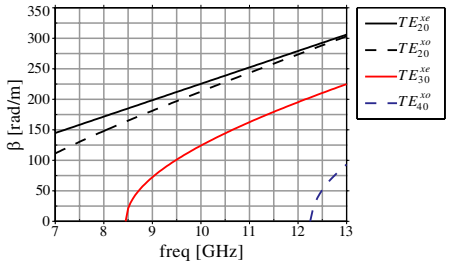

Figure 3. Dispersion diagram of the E-plane loaded rectangular waveguide in the X-band.

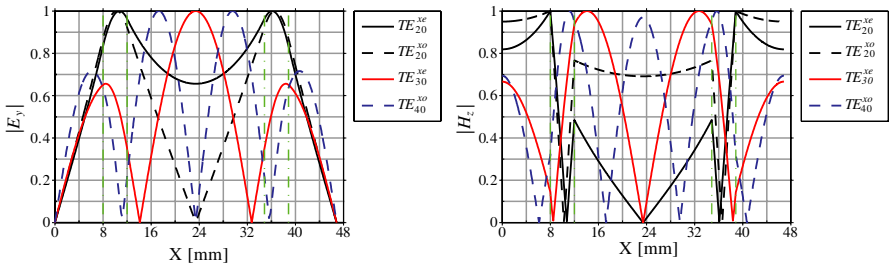

Figure 4. Normalized field distribution of the first TE^x modes in the E-plane loaded rectangular waveguide in the X-band (green-dashed lines indicate limits of dielectric slabs). (a) Electric field (E_y). (b) Magnetic field (H_z).

The field distribution of mode TE_{30}^{xe} is specially important since it allows the confinement of most of the energy in the central region of air by suitably choosing the waveguide dimensions and the width and position of the dielectric slabs. By doing so, total losses may be decreased enabling a low-loss waveguide. Next section deals with the way in which losses may be analytically obtained and Section 4 proposes an optimization procedure for the dielectric slabs.

3. LOSSES ON LOADED WAVEGUIDE

The attenuation in the E-plane loaded rectangular waveguide is caused by losses on the outer conductor and in the dielectric slabs. Both can be easily determined from the electric and magnetic field expressions shown in Equations (5)–(9). This section is devoted to the analytical determination of these losses.

Ohmic losses on the outer metallic surface cause an attenuation (α_c) that can be computed by means of the following expression [22]:

$$\alpha_c = \frac{P_{lc}}{2P_0} \tag{16}$$

where P_0 is the power transmitted by the waveguide determined as follows:

$$P_0 = \frac{1}{2}\Re\mathrm{e} \oint_S \vec{E} \times \vec{H}^* d\vec{s} \tag{17}$$

and P_{lc} is the power dissipated in ohmic losses per unit length of the metallic walls. This power can be obtained as:

$$P_{lc} = \frac{R_s}{2} \int_S |\vec{H}_t|^2 ds \tag{18}$$

where R_s is the surface resistance computed as $R_s = \sqrt{\omega\mu/(2\sigma)}$.

The dielectric slabs dissipate power due to the absorption of energy. The additional attenuation caused by this dissipation can be computed as:

$$\alpha_d = \frac{P_{ld}}{2P_0} \tag{19}$$

where P_{ld} is the power dissipated in dielectric slabs per unit length given by:

$$P_{ld} = \frac{\omega\varepsilon''}{2} \int_V |\vec{E}|^2 dV \tag{20}$$

being $\varepsilon'' = \varepsilon_r\varepsilon_0 \tan\delta$. Note that the field used in these expressions is the solution of the loss-free case (5)–(9), which is a common solution in the perturbational method.

The conductor (α_c) and dielectric (α_d) attenuations have been computed for the example presented in previous section. Fig. 5 shows the obtained attenuation considering copper for the metallic walls and dielectric slabs with permittivity $\varepsilon_r = 2.2$ and loss tangent $\tan\delta = 0.001$.

From Fig. 5, it can be clearly seen that all modes present higher dielectric losses than conductor losses, but this trend is increased in modes TE_{20}^{xe} and TE_{20}^{xo}. This is because these modes concentrate most of power in the dielectric slabs, as shown in Fig. 4.

Furthermore, from Fig. 5, it also can be concluded that the best trade-off between conductor and dielectric losses takes place in mode TE_{30}^{xe}. This mode confines most of power in the central region of air. Consequently, ohmic losses are mainly produced by the upper and lower central conductors and, hence, conductor losses remain moderately low. Also, dielectric losses are lower than in other modes

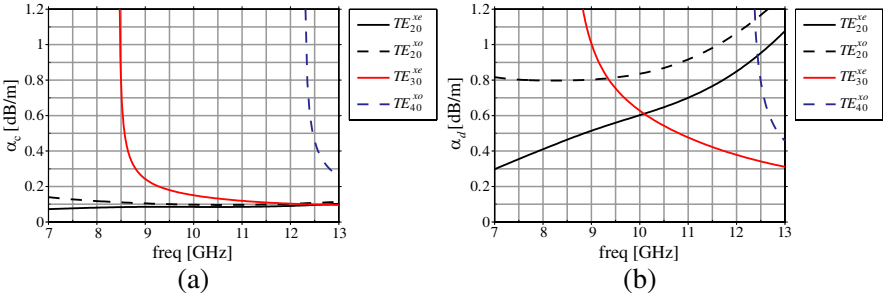

Figure 5. Conductor and dielectric attenuation in the E-plane loaded rectangular waveguide. (a) Conductor losses (α_c). (b) Dielectric losses (α_d).

because the dielectric absorption only takes place in the small portion of power transmitted to the dielectric slabs.

Probably, the most important drawback to work with mode TE_{30}^{xe} is the fact of not being the fundamental mode. However, since modes TE_{20}^{xe} and TE_{20}^{xo} are only present in the dielectric slabs, mode TE_{30}^{xe} can be easily excited without exciting modes TE_{20}^{xe} and TE_{20}^{xo}. Also, there is a great bandwidth between this mode and the next mode, TE_{40}^{xo} (see Fig. 3). Therefore, all along this bandwidth, bends and discontinuities will not excite any high-order mode, since they are all below cut-off.

Although mode TE_{30}^{xe} is the best choice to operate, it must be taken into account that the presented waveguide is not optimized. Focusing our attention on this mode, dielectric slabs may be optimized to reduce the total attenuation of the mode. The first option consists in optimizing the dielectric slabs applying the previously presented method. Nevertheless, the determination of the propagation constants for every considered slabs' size using (11) and (12) requires a high computation time. To speed-up the optimization, next section proposes a faster algorithm.

4. DIELECTRIC SLAB OPTIMIZATION

As commented above, the attenuation of mode TE_{30}^{xe} is caused by, both, ohmic losses and dielectric losses. In order to reduce this attenuation, the position and dimensions of lateral dielectric slabs must be optimized to maximize the confinement of TE_{30}^{xe} mode in the central region of air. This optimization is carried out considering the rectangular metallic waveguide as a reference.

By looking at Fig. 4(a), and taking into account that $E_z = 0$

for TE_{30}^{xe} mode, it is clear that this mode looks like the fundamental mode (TE_{10}^{z}) in a common rectangular metallic waveguide. They both have the same polarization and the same cosine-like distribution in the central region. The difference lies in the lateral walls: whereas TE_{10}^{z} mode is limited on laterals by a metallic surface, which makes E_y vanish on these surfaces; TE_{30}^{xe} mode in the E-plane loaded rectangular waveguide is just confined by dielectric slabs, what causes the field to partially flow to the lateral regions.

Therefore, the waveguide under study may be considered as a special case of a rectangular metallic waveguide with lateral metallic walls substituted by a multilayer structure. This structure is formed by the dielectric slabs and the outer lateral air regions (regions 1 and 2, and 4 and 5, in Fig. 1). Hence, the maximization of power confinement in TE_{30}^{xe} mode must determine not only the dimensions of the dielectric slabs, but also the width of the outer lateral air regions, i.e., the complete lateral multilayer structure must be considered to this aim.

The maximum confinement of mode TE_{30}^{xe} is achieved by enforcing an electric wall boundary condition in the interface between the central region and the multilayer lateral structure. By doing so, a total reflection condition is obtained. This kind of reflection may be better studied from the point of view of a plane wave impinging on the multilayer lateral structure. To start with this study, the behaviour of the rectangular waveguide must be first reviewed.

The fundamental mode of a rectangular metallic waveguide (TE_{10}^{z}) may be studied as two plane waves with an oblique incidence on side walls [**?**], as shown in Fig. 6. The interference of these two plane waves causes the sinusoidal variation of the TE_{10}^{z} mode on the transversal plane. In the vertical direction (y), the electric field is invariant because both plane waves propagate parallel to the upper and lower walls. The angle of incidence (θ) may be obtained from the propagation constant

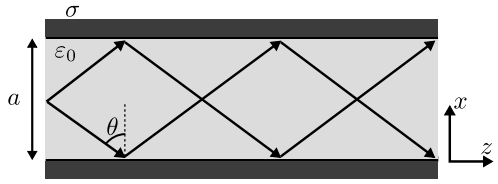

Figure 6. Decomposition of the fundamental mode into two plane waves, in a metallic rectangular waveguide.

(β) as:

$$\theta = \arccos\left(\frac{\beta}{k}\right) \tag{21}$$

To keep the same field distribution in both, the rectangular metallic waveguide and the E-plane loaded rectangular waveguide, the same plane waves concept may be considered. Fig. 7 depicts a longitudinal top view of the E-plane loaded rectangular waveguide with mode TE_{30}^{xe} decomposed into two plane waves in the central region of air. Since it is desired the same field distribution in modes TE_{10}^{z} and TE_{30}^{xe}, it may be assumed the same propagation constant for both modes. Therefore, the angle of incidence in Fig. 7 coincide with that of the rectangular metallic waveguide of Fig. 6, provided that $a = w_{a0}$.

The above decomposition allows the easy optimization of the dielectric slabs by just considering the reflection of a plane wave on the multilayer structure. This is because only half of the structure in Fig. 7 needs to be considered due to the symmetry of the problem. Thus, the optimization problem may be simplified to the one depicted in Fig. 8. As can be observed, the incidence of a single plane-wave is considered. The material of the first and third layers (the central and outer air regions in the original problem) is air (ε_0), whereas the second layer (the dielectric slabs) is characterized by the permittivity ε_r.

The determination of the optimal w_d and w_{a1} widths considers the

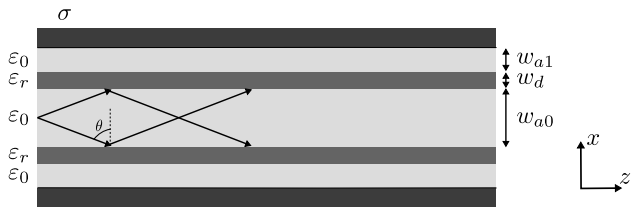

Figure 7. Decomposition into two plane waves of the TE_{30}^{xe} mode in the E-plane loaded rectangular waveguide.

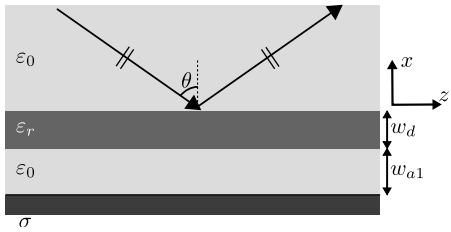

Figure 8. Incidence of a plane wave on a 2-layer structure.

reflection on the final metallic surface as well as the multiple reflections in the intermediate layers. All these reflections may be characterized by the matrix multiplication shown in [23] or in [24]. Nevertheless, for the sake of simplicity, in this paper the *generalized reflection coefficient* of the multilayer structure [25] is considered. This coefficient can be determined, for a TE incidence, as:

$$\tilde{R}_{TE}^{n+1,n} = \frac{R_{TE}^{n+1,n} + \tilde{R}_{TE}^{n,n-1} e^{-j2w_n k_{x_n}}}{1 + R_{TE}^{n+1,n} \tilde{R}_{TE}^{n,n-1} e^{-j2w_n k_{x_n}}} \tag{22}$$

where the superindices indicate the layers between which the reflection coefficient is computed, starting from $n = 3$ for the upper layer (the central air region) and ending in layer $n = 0$ for the lower metallic layer (surrounding conductor in the original waveguide). Parameter w_n is the width of layer n ($w_2 = w_d$ and $w_1 = w_{a1}$) and k_{x_n} is the wavevector along the x-direction in the nth-layer. Coefficients R_{TE}^{mn}, known as *Fresnel coefficients*, represent the reflection produced by an individual dielectric discontinuity and are given by

$$R_{TE}^{mn} = \frac{k_{x_m} - k_{x_n}}{k_{x_m} + k_{x_n}} \tag{23}$$

Once the generalized reflection coefficient at each interface is known, the *generalized transmission coefficient* from any layer to the lower conductor medium ($\tilde{T}_{TE}^{N0}$) can be easily determined by means of the following expression:

$$\tilde{T}_{TE}^{N0} = \prod_{n=0}^{N-1} S^{n+1,n} e^{-jw_{n+1}k_x^{n+1}} \tag{24}$$

where

$$S^{n+1,n} = \frac{T_{TE}^{n+1,n}}{1 + R_{TE}^{n+1,n} \tilde{R}_{TE}^{n,n-1} e^{-j2w_n k_{x_n}}} \tag{25}$$

The optimization process determines the widths w_d and w_{a1} that minimize the coefficient $\tilde{T}_{TE}^{30}$, i.e., the power transmitted from the first layer ($n = 3$, the central region of air) to the metallic medium. By doing so, ohmic losses are minimized and the power transmitted to the dielectric slabs is considerably reduced, increasing the field confinement.

Results

The E-plane loaded rectangular waveguide shown in Section 2 has been optimized at 10 GHz. The central region dimensions of this waveguide

are $w_{a0} = 22.86\,\text{mm}$ and $h = 10.16\,\text{mm}$. The propagation constant of the fundamental mode in the equivalent rectangular metallic waveguide is $\beta = 158.25\,\text{rad/m}$. From this propagation constant, the angle of incidence determined with (21) is $\theta = 49.08°$.

Figure 9(a) shows the transmission coefficient $\tilde{T}_{TE}^{30}$ computed with (24) for different widths w_d and w_{a1}. From this figure, it can be easily deduced the combination of widths w_d and w_{a1} that give the minimum transmission coefficient. In this example, the optimized widths are: $w_d = 5.87\,\text{mm}$ and $w_{a1} = 11.44\,\text{mm}$.

The dispersion diagram of the optimal E-plane loaded rectangular waveguide has been computed with (11) and (12). The result is shown in Fig. 9(b). As can be observed, now, a higher number of modes propagate along the optimized waveguide. However, it must be noted that, from 7 to 10 GHz, there are only three propagating modes: TE_{20}^{xe},

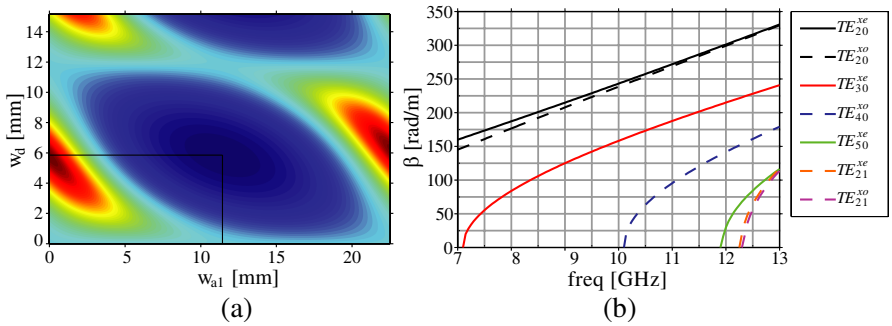

Figure 9. Optimization of the multilayer structure and dispersion diagram in the optimized waveguide. (a) Transmission coefficient. (b) Dispersion diagram.

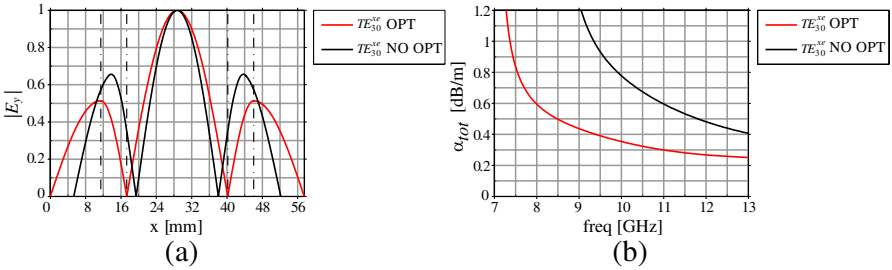

Figure 10. Comparison of TE_{30}^{xe} mode in the optimized and non-optimized E-plane loaded rectangular waveguide. (a) Electric field (E_y) cross section. (b) Total losses.

TE_{20}^{xo} and TE_{30}^{xe}.

Figure 10(a) compares the electric field distribution of mode TE_{30}^{xe} in the optimized waveguide and in the non-optimized waveguide (described in Section 2). As it was desired, the optimized mode presents a higher confinement than the non-optimized mode. Also, in the optimized design, the field completely vanishes in the interface between the central region and the dielectric slabs, and lateral lobes are lower than in the non-optimized design (note that dashed lines indicate limits of regions in the optimized design).

Since the electric and magnetic field of the optimized mode decrease in lateral regions, and power is confined in the central region of air, both conductor and dielectric losses decrease. Fig. 10(b) shows a comparison of total losses ($\alpha_{tot} = \alpha_c + \alpha_d$) in the optimized and non-optimized waveguides. From this comparison, it may be concluded that a considerably reduction in total losses is achieved at the frequency of interest by means of the proposed optimization.

5. PRACTICAL RESULTS

The E-plane loaded rectangular waveguide has been fabricated to proof the validity of the proposed optimization algorithm. The prototype has been designed to work in the Ka-band. The dimensions of the standard WR-28 waveguide ($7.112\,\text{mm} \times 3.556\,\text{mm}$) have been used for the central region of air. The material for the lateral dielectric layers is the Arlon's substrate AD1000, with permittivity $\varepsilon_r = 10.2$ and $\tan\delta = 0.0025$. The optimization of lateral layers gives the following dimensions: $w_d = 0.78\,\text{mm}$ and $w_{a1} = 3.57\,\text{mm}$.

A 3D-view of the manufactured prototype is shown in Fig. 11. Note that, in this picture, the upper metallic wall has been removed to be able to observe the internal E-plane loaded structure. In these pictures, it can be seen the internal air region confined by the vertical dielectric slabs and the outer air regions. The conductor used for the outer metallic walls is Aluminum ($\sigma = 3.8 \times 10^7\,\text{S/m}$).

The internal configuration may be better observed in Fig. 12. Here, it can be seen the wider central region of air and the lateral dielectric and air regions. The transition from the WR-28 waveguide to the E-plane loaded waveguide may be observed on input and output ports. This transition injects directly the fundamental mode of the feeding rectangular waveguide into the central region of air in the proposed waveguide, taking advantage of the similar field distribution in both cases.

The optimized E-plane loaded rectangular waveguide has been simulated with Ansys HFSS [26]. Fig. 13(a) depicts the simulated

structure, including the input and output transitions. Fig. 13(b) shows the electric field in the waveguide on a longitudinal section at 30.5 GHz. As can be observed, the electric field is mostly confined inside the central region of air.

The S-parameters of the fabricated prototype have been measured and compared to simulations. Fig. 14 shows the comparison for both, the S_{11} and S_{21} parameters. In Fig. 14(a) it can be seen that the measured S_{11} parameter is quite similar to the simulated one. Despite the measured S_{11} is a bit higher than the simulated S_{11} parameter, measurements are below -20 dB in all the band.

In Fig. 14(b), measured and simulated S_{21} parameters are compared. From this figure it can be concluded that measured results confirm the simulated predictions. The measured transmission coefficient presents a variation of less than 0.4 dB caused by the effect of transitions. The most important result, however, is the fact that losses are quite low due to the power confinement in the central air region. Considering the total length of the waveguide (11 cm) and the losses introduced by the input and output transitions, an attenuation of around 0.03 dB/cm may be determined from results in Fig. 14.

6. E-PLANE LOADED RECTANGULAR WAVEGUIDE AT HIGH FREQUENCIES

The E-plane loaded rectangular waveguide presents valuable features at low frequencies due to the strong confinement of field in the central region of air [3, 4]. Also, if a low-loss dielectric is used, total attenuation of the waveguide may be lower than the attenuation of a rectangular waveguide. This improvement is particularly significant at high frequencies, e.g., in the submillimeter-wave band or in the THz band.

At these frequencies, conductors present high skin-depth losses

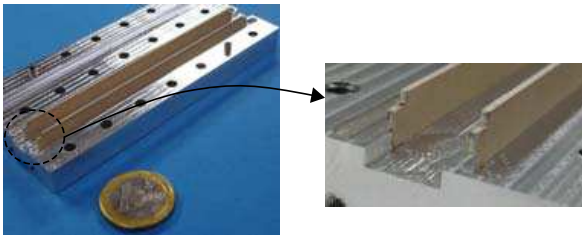

Figure 11. E-plane loaded rectangular waveguide fabricated in the Ka-band.

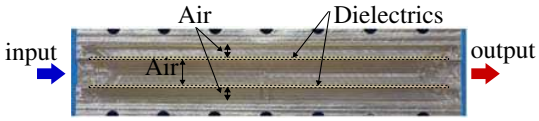

Figure 12. Top view of the E-plane loaded rectangular waveguide fabricated in the Ka-band.

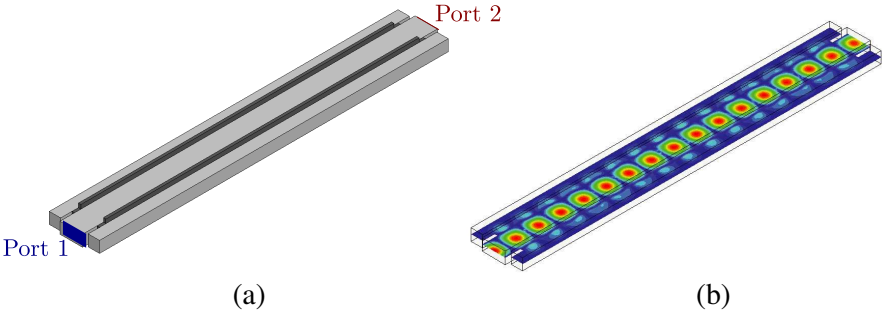

Figure 13. Optimized E-plane loaded waveguide simulated with HFSS. (a) Simulated prototype. (b) Simulated electric field.

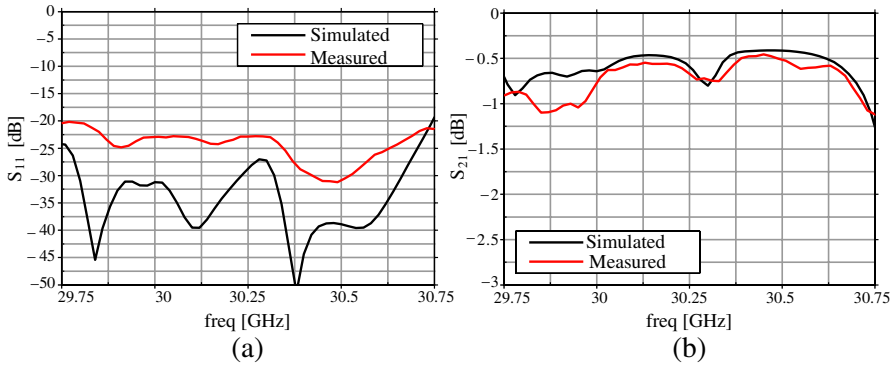

Figure 14. Comparison of simulated and measured (a) S_{11} and (b) S_{21} parameters in the fabricated E-plane loaded waveguide in the Ka-band.

and dielectrics have a high power absorption [11], which increases the attenuation of any waveguide [12]. This makes common waveguides, e.g., the metallic rectangular or circular waveguides, impractical.

Several low-loss waveguides have been proposed to solve this problem, e.g., the dielectric circular waveguide [27], the elliptical

polymer tube [28], the Ribbon waveguide [29] or the single-wire waveguide [30]. All these waveguides present low attenuation at high frequencies, but are affected by high losses on bends and discontinuities.

The E-plane loaded rectangular waveguide may solve these problems while keeping the attenuation below those of common waveguides at high frequencies. This improvement is similar to that of the metallo-dielectric EBG waveguide [11], where the energy is also confined by a multilayer structure, but in a circular waveguide. The main advantage of the waveguide under study lies in the rectangular shape of the waveguide, suitable to easily design and manufacture devices and antennas.

The proposed optimization algorithm has been used to design the E-plane loaded rectangular waveguide at 1 THz. The dimensions of the central region of air are 240 µm × 120 µm. The materials used for the lateral layers are: high resistivity silicon ($\varepsilon_r = 11.58$ and $\tan\delta = 0.0003$ at 1 THz) [31] for the dielectric slabs (regions $r = 2$ and $r = 4$) and air ($\varepsilon_r = 1$) for the outer layers (regions $r = 1$ and $r = 5$). The optimized dimensions, according to Fig. 1 notation, are: $w_d = 22.66\,\mu\text{m}$ and $w_{a1} = 120.48\,\mu\text{m}$.

The resulting structure has been simulated with Ansys HFSS [26]. Fig. 15 shows both, the structure and the electric field distribution in the waveguide. As in previous designs, the energy is mainly confined in the central region of air.

The total attenuation of the optimized E-plane loaded rectangular waveguide at 1 THz assuming a gold shielding ($\sigma = 4.098 \times 10^7\,\text{S/m}$, shown in Fig. 15(a) as a red sheet) is 0.7 dB/cm, which means a 33% reduction with regard to the attenuation of a fully metallic

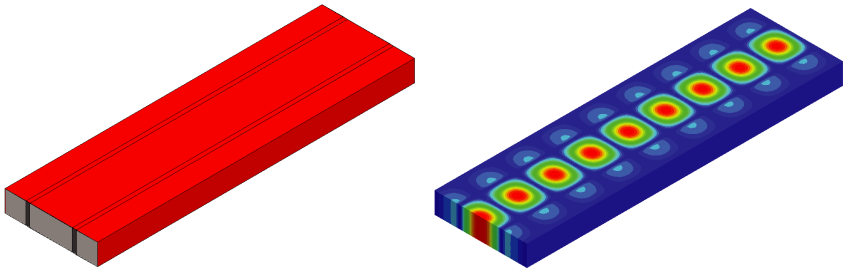

Figure 15. E-plane loaded rectangular waveguide at THz frequencies. (a) Structure. (b) Electric field.

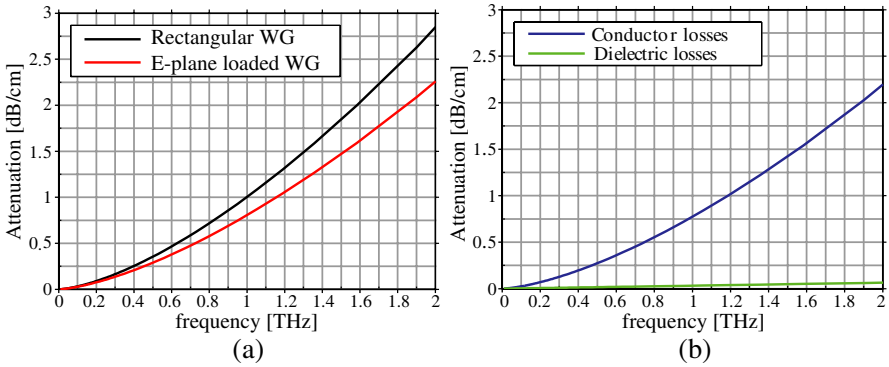

Figure 16. Attenuation of the E-plane loaded rectangular waveguide optimized at 1 THz and scaled at different frequencies. (a) Total attenuation. (b) Partial attenuation in the proposed waveguide.

rectangular waveguide ($\alpha = 0.91$ dB/cm) with the same dimensions (240 µm × 120 µm).

The optimized design has been scaled at different frequencies keeping the same dielectric material (high resistivity silicon). The aim is to know the frequency at which the optimized E-plane loaded rectangular waveguide presents lower losses than a conventional rectangular waveguide with the same internal dimensions. Fig. 16(a) shows the comparison between these two waveguides. From this figure it may be concluded that the higher the frequency, the larger the reduction of attenuation in the optimized E-plane loaded rectangular waveguide. In addition, although it cannot be clearly seen in Fig. 16(a), a study of this comparison at low frequencies lets us conclude that the proposed waveguide presents lower losses than the equivalent rectangular metallic waveguide from 20 GHz on.

Losses are jointly produced by the outer metallic walls and the dielectric materials. However, by looking at Fig. 16(b) it can be clearly seen that, since a low-loss dielectric is used, the dielectric attenuation is extremely low, and the main contribution to the total losses comes from the conductor, which are located on the upper and lower metallic walls of the central region of air. If a higher reduction of losses is desired, attention should be focused on the elimination of these losses, though this study is beyond the scope of this paper.

Finally, it is worth noting that the E-plane loaded rectangular waveguide may be bent or used to efficiently design devices. This possibility becomes specially important at high frequencies, where devices are hardly designed with any other kind of waveguide due to

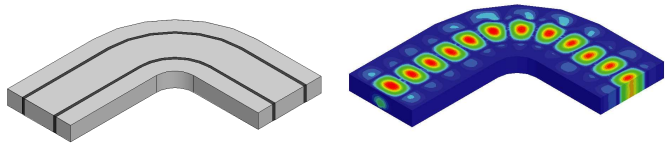

Figure 17. 90° bend on the E-plane loaded rectangular waveguide. (a) Structure. (b) Electric field.

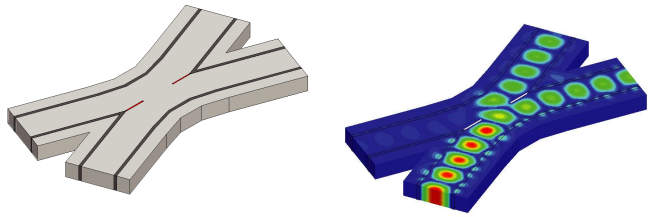

Figure 18. Coupler designed with the E-plane loaded rectangular waveguide. (a) Structure. (b) Electric field.

technology problems or high losses.

Figure 17 shows a curve in the E-plane loaded rectangular waveguide at 1 THz (outer metallic shielding is omitted in the picture to show the internal configuration). In this figure, it can be clearly seen that field is completely confined along the curve and a very low coupling is produced to other modes. From this behaviour it may be assumed a quite good performance in using the proposed waveguide to design other types of devices, e.g., power dividers or power distributors.

Figure 18 shows a directional coupler designed with the optimized E-plane loaded rectangular waveguide (outer metallic shielding is again omitted to show the internal configuration). In Fig. 18(a), red slabs are metallic walls inserted to adjust the coupling between the different ports (clockwise from the lower port: input, isolated, coupled and through). Fig. 18(b) shows the electric field in the coupler where, as can be observed, the field is correctly distributed from the input to the coupled and through ports. The behaviour of this coupler is similar to

a quadrature hybrid at 1 THz, with a directivity of 17 dB, a coupling factor of 3.73 dB, and 3.45 dB of insertion losses, with a bandwidth for these parameters of 10%. These results show the wide range of possibilities that an optimized E-plane loaded rectangular waveguide may offer.

7. CONCLUSIONS

The E-plane loaded rectangular waveguide with symmetrical dielectric slabs has been analytically studied. The attention has been focused on the study of TE^x modes, the lower-order modes of this waveguide. By looking at the power distribution of these modes, interesting characteristics have been found for one of them, the TE_{30}^{xe} mode which, despite not being the fundamental mode, confines the energy in the central air region.

This paper proposes a method to optimize the lateral layers in the E-plane loaded rectangular waveguide. The aim of the method is to maximize the power confinement of TE_{30}^{xe} mode in the central region and, hence, reduce its attenuation. The proposed optimization is faster than the analytical optimization of the waveguide since the computation of propagation constants and the integration of field are avoided.

Results show the reduction of attenuation of mode TE_{30}^{xe} in the optimized waveguide. These results have been tested in a practical case. Measurements let us conclude that the proposed procedure gives quite good results according to the high power confinement simulated with HFSS and the high similarity between simulated and measured S_{21} parameter.

Finally, the good behaviour of the waveguide at THz frequencies has been pointed out. At these frequencies, the proposed procedure not only allows the maximization of power confinement, but also allows the design of waveguides with lower losses than conventional waveguides. This fact, in conjunction with its good behaviour on bends, opens new possibilities for the design of practical low-loss waveguides at THz frequencies and for the design of efficient devices at these frequencies.

ACKNOWLEDGMENT

This work has been supported by the Spanish Ministry of Science and Innovation (Ministerio de Ciencia e Innovación) under the projects TEC2010-20841-C04-01 and CSD2008-00068.

REFERENCES

1. Collin, R. E., *Field Theory of Guided Waves*, John Wiley & Sons, 1991.
2. Harrington, R. F., *Time-Harmonic Electromagnetic Fields*, John Wiley & Sons, 2001.
3. Tsandoulas, G., D. Temme, and F. Willwerth, "Longitudinal section mode analysis of dielectrically loaded rectangular waveguides with application to phase shifter design," *IEEE Transactions on Microwave Theory and Techniques*, Vol. 18, No. 2, 88–95, 1970.
4. Bogle, A., M. Havrilla, D. Nyquis, L. Kempel, and E. Rothwell, "Electromagnetic material characterization using a partially-filled rectangular waveguide," *Journal of Electromagnetic Waves and Applications*, Vol. 19, No. 10, 1291–1306, 2005.
5. Seckelmann, R., "Propagation of te modes in dielectric loaded waveguides," *IEEE Transactions on Microwave Theory and Techniques*, Vol. 14, No. 11, 518–527, 1966.
6. Witt, H., R. Biss, and E. Price, "Propagation constants of a waveguide containing parallel sheets of finite conductivity," *IEEE Transactions on Microwave Theory and Techniques*, Vol. 15, No. 4, 232–239, 1967.
7. Gardiol, F., "Higher-order modes in dielectrically loaded rectangular waveguides," *IEEE Transactions on Microwave Theory and Techniques*, Vol. 16, No. 11, 919–924, 1968.
8. Simons, R., "On mode classification in rectangular waveguides partially filled with dielectric slabs," *IEEE Transactions on Microwave Theory and Techniques*, Vol. 34, No. 2, 297–298, 1986.
9. Bui, V. and R. Gagne, "Dielectric losses in an H-plane-loaded rectangular waveguide (short papers)," *IEEE Transactions on Microwave Theory Techniques*, Vol. 20, No. 9, 621–623, 1972.
10. Jiang, Z., Z. Shen, and X. Shan, "Mode-matching analysis of waveguide T-junction loaded with an H-plane dielectric slab," *Journal of Electromagnetic Waves and Applications*, Vol. 16, No. 11, 1613–1614, 2002.
11. Llombart, N., A. Mazzinghi, P. Siegel, and A. Freni, "Design of a low loss metallo-dielectric EBG waveguide at submillimeter wavelengths," *IEEE Microwave and Wireless Components Letters*, Vol. 19, No. 7, 437–439, 2009.
12. Wang, Z., L. Ye, Y. Zhang, R. Xu, and W. Lin, "Investigation of terahertz wave propagation along parallel-plate dielectric waveguide using various metal conductivity models," *Journal of*

Electromagnetic Waves and Applications, Vol. 8, No. 9, 1231–1242, 2011.

13. Matvejev, V., C. de Tandt, W. Ranson, J. Stiens, R. Vounckx, and D. Mangelings, "Integrated waveguide structure for highly sensitive THz spectroscopy of nano-liter liquids in capillary tubes," *Progress In Electromagnetics Research*, Vol. 121, 89–101, 2011.
14. Xu, O., "Diagonal horn Gaussian efficiency enhancement by dielectric loading for submillimeter wave application at 150 GHz," *Progress In Electromagnetics Research*, Vol. 114, 177–194, 2011.
15. Zhu, B., J. Stiens, V. Matvejev, and R. Vounckx, "Inexpensive and easy fabrication of multi-mode tapered dielectric circular probes at millimeter wave frequencies," *Progress In Electromagnetics Research*, Vol. 126, 237–254, 2012.
16. Tayeboun, F., R. Naoum, H. Tayeboun, H. Hattori, and F. Salah-Belkhodja, "Improved transmission waveguide bends in photonic crystal," *Journal of Electromagnetic Waves and Applications*, Vol. 19, No. 5, 615–628, 2005.
17. Tretyakov, O. A. and M. Kaya, "The real-valued time-domain TE-modes in lossy waveguides," *Progress In Electromagnetics Research*, Vol. 127, 405–426, 2012.
18. Canto, J. R., C. P. Paiva, and A. M. Barbosa, "Modal analysis of bi-isotropic H-guides," *Progress In Electromagnetics Research*, Vol. 111, 1–24, 2011.
19. Dong, J., J. Li, and F.-Q. Yang, "Guided modes in the four-layer slab waveguide containing chiral nihility core," *Progress In Electromagnetics Research*, Vol. 112, 241–255, 2011.
20. Choudhury, P. K., "Transmission through twisted clad liquid crystal optical fibers," *Progress In Electromagnetics Research*, Vol. 131, 169–184, 2012.
21. Dong, J. and J. Li, "Characteristics of guided modes in uniaxial chiral circular waveguides," *Progress In Electromagnetics Research*, Vol. 124, 331–345, 2012.
22. Pozar, D., *Microwave and RF Design of Wireless Systems*, John Wiley & Sons, Inc., New York, NY, USA, 2000.
23. Pei, Y., A. Zeng, L. Zhou, R. Zhang, and K. Xu, "Electromagnetic optimal design for dual-band radome wall with alternating layers of staggered composite and kagome lattice structure," *Progress In Electromagnetics Research*, Vol. 122, 437–452, 2012.
24. Francés Monllor, J., C. Neipp, A. Marquez Ruiz, A. Belendez, and I. Pascual, "Analysis of reflection gratings by means of a

matrix method approach," *Progress In Electromagnetics Research*, Vol. 118, 167–183, 2011.

25. Chew, W., *Waves and Fields in Inhomogenous Media*, IEEE Press, Piscataway, NJ, 1995.
26. Corporation, A., "HFSS (high frequency structural simulator)," Suite v11, Pittsburg, PA, USA, 2009.
27. Jamison, S., R. McGowan, and D. Grischkowsky, "Single-mode waveguide propagation and reshaping of sub-ps terahertz pulses in sapphire fibers," *Applied Physics Letters*, Vol. 76, 1987, 2000.
28. Chen, D. and H. Chen, "Highly birefringent low-loss terahertz waveguide: Elliptical polymer tube," *Journal of Electromagnetic Waves and Applications*, Vol. 11, No. 12, 1553–1562, 2010.
29. Yeh, C., F. Shimabukuro, and P. Siegel, "Low-loss terahertz ribbon waveguides," *Applied Optics*, Vol. 44, No. 28, 5937, 2005.
30. Wang, K. and D. Mittleman, "Metal wires for terahertz wave guiding," *Nature*, Vol. 432, No. 7015, 376–379, 2004.
31. Bolivar, P., M. Brucherseifer, J. Rivas, et al., "Measurement of the dielectric constant and loss tangent of high dielectric-constant materials at terahertz frequencies," *IEEE Transactions on Microwave Theory and Techniques*, Vol. 51, No. 4, 1062–1066, 2003.